Materials Science and Engineering, 51 (1981) 47 - 53

Room Temperature Decomposition of a Superplastic Zn–Al Eutectoid Alloy

FU-WEN LING*

Product Research and Development Department, St. Joe Minerals Corporation, Monaca, PA 15061 (U.S.A.)

DAVID E. LAUGHLIN

Department of Metallurgical Engineering and Materials Science, Carnegie–Mellon University, Pittsburgh, PA 15213 (U.S.A.)

S. C. CHANG

Department of Physics, Duquesne University, Pittsburgh, PA 15219 (U.S.A.)

(Received January 16, 1981; in revised form May 4, 1981)

SUMMARY

In this paper the room temperature decomposition behavior of a commercial Zn–Al alloy is described. In particular, the build-up of internal strain is documented by an X-ray line-broadening technique, and the corresponding transmission electron microscopy microstructures are presented and discussed. Also presented is the room temperature mechanical behavior of the alloys, as a function of natural aging time. These properties are correlated with and interpreted in terms of the internal strain and microstructure. The results of this work lead to some rather important recommendations as to the processing and application of this alloy.

1. INTRODUCTION

The binary Zn–Al eutectoid alloy exhibits superplastic behavior at elevated temperatures after it has decomposed at room temperature, after quenching from above the eutectoid temperature. Water-quenched specimens, after such a transformation, consist of extremely fine grains (about 1 μm) of α (aluminum-rich) phases and β (zinc-rich) phases with incoherent interphase interfaces or grain boundaries. These fine grains with incoherent boundaries contribute to the superplastic behavior.

However, the binary Zn–Al alloys possess poor mechanical properties at room temperature. Therefore Zn–Al alloys are usually alloyed with copper and magnesium to improve the room temperature tensile and creep strengths for commercial use. As a result of the alloy additions, the rate of room temperature decomposition is significantly retarded. For example, after quenching from above the eutectoid temperature, the binary alloy completely transforms into a two-phase $\alpha + \beta$ mixture within a few minutes, whereas it takes a few weeks for alloys with only a small magnesium addition, *e.g.* 0.001 wt.% [1]. This profound effect on transformation kinetics is attributed to the retardation of diffusion due to the trapping of vacancies by magnesium atoms [2, 3] which are slightly larger than aluminum and zinc.

The alloy additions greatly affect the superplastic behavior. Alloys containing magnesium cannot be produced with superplastic properties by heat treatment alone; a thermomechanical process is required to obtain superplastic behavior [4]. The reason for this is that the alloys containing magnesium exhibit a *coherent* two-phase structure when decomposed at room temperature. This coherency persists even when the alloys are heat treated for prolonged times at various temperatures [5]. Deformation is required to destroy the coherency and therefore to produce incoherent grain boundaries which enable the alloy to deform superplastically (see ref. 1 for a discussion of this).

Another difficulty that has been observed is that the semicontinuously cast slabs of alloys containing magnesium tend to crack during room temperature aging. This cracking is

*Present address: Materials Science, Revere Research Inc., P.O. Box 1352, Edison, NJ 08837, U.S.A.

0025-5416/81/0000-0000/$02.50

caused by the considerable internal stress produced by the alloys when they are decomposed at room temperature. This stress is of course due to the persistence of coherency. In this study the grain size and internal strain were measured using the X-ray line-broadening technique and transmission electron microscopy (TEM) on samples aged for various times after water quenching. These data were then used to interpret the observed room temperature mechanical behavior of the alloys.

2. EXPERIMENTAL DETAILS

A commercial sheet product 0.060 in (1.52 mm) thick was used in this experiment. Wet chemical analysis of these samples showed that they had the following composition: 22.0% Al, 0.035% Mg, 0.026% Ca and the balance zinc.

For X-ray diffraction and TEM studies, samples 25 mm × 25 mm were solution heat treated at 350 °C for 20 h and water quenched. Both X-ray and TEM studies were conducted at various times after quenching. TEM was carried out on a JEOL-100B microscope operating at 100 kV. A double-tilt stage with tilting capabilities of ±60° was utilized.

2.1. Line-broadening analysis

The X-ray line-broadening technique described by Taylor [6] was used to determine the grain size and internal stress. The separation of particle size broadening (actually, in this case, the grain size) from internal strain broadening is possible because the two types of broadening vary in different ways with the reflection angle θ. The combined effect of particle size broadening and strain broadening can be described by

$$B = B_{\text{grain size}} + B_{\text{strain}}$$

i.e. by

$$B = \frac{\lambda}{\epsilon \cos\theta} + \frac{4\bar{\sigma}}{E_{hkl}} \tan\theta$$

where B is the line breadth, ϵ is the particle or grain size, $\bar{\sigma}$ is the mean stress, λ is the X-ray wavelength, E_{hkl} is Young's modulus in the $[hkl]$ crystallographic direction and θ is the reflection angle.

The equation can be written in the form

$$\frac{B \cos\theta}{\lambda} = \frac{1}{\epsilon} + \frac{4\bar{\sigma}}{\lambda E_{hkl}} \sin\theta$$

Thus from the line breadths B of several reflections, a plot of $(B \cos\theta)/\lambda$ against $(\sin\theta)/\lambda$ should be a straight line. The intercept on the $(B \cos\theta)/\lambda$ axis will yield $1/\epsilon$, while the slope may be used to calculate mean stress $\bar{\sigma}$.

This technique is particularly useful when many reflection lines are available for plotting. Since a total of nine reflections from both α and β were used, the parameters determined by linear regression analysis were statistically quite significant. It should be noted that reflections from the α phase could not be used during the early stage of the transformation, because of overlapping with the α' phase reflections.

This technique was used to estimate the crystallite size and the internal stress of the sheet sample after solutionizing at 350 °C for 20 h and water quenching. A powder sample, filed from the as-received commercial product and annealed at 120 °C for 2 days, was used for instrumental correction. The breadth of the reflection lines was measured from the chart. The scanning speed used in this experiment was 0.2° (2θ) min^{-1}.

2.2. Volume fraction measurements

The rate of eutectoid decomposition at room temperature was studied by X-ray diffraction. The volume fraction measurements were performed at various times after quenching. To eliminate the texture error, a powder sample was used. The powder sample was wrapped in molybdenum foil, solution treated at 350 °C for 4 h and water quenched. The integrated intensities of the following non-overlapping reflections were used for calculation: $(10\bar{1}1)_\beta$, $(220)_\alpha$, $(220)_{\alpha'}$ and $(10\bar{1}3)_\beta$. The integrated intensity of these reflections from a fully transformed sample was used for normalization.

2.3. Mechanical tests

Tensile specimens were made with a gauge length of 2 in. They were heat treated at 350 °C for 20 h, followed by a water quench. Tensile tests were conducted on an Instron testing machine using a strain rate of 0.2 min^{-1}. The changes in hardness after quenching were also examined by hardness tests at various times, using a Rockwell B scale with a 30 s indentation time.

3. RESULTS

3.1. Volume fraction measurement

Figure 1 shows a plot of $\log[\ln\{1/(1-\zeta)\}]$ against $\log t$ where ζ is the fraction of β phase formed and t is the aging time at room temperature after the water quench. The slope of this plot yields the n value of the Avrami equation:

$$\zeta = 1 - \exp(-Kt^n)$$

The n value, in conjunction with the microstructure, may be used to understand the transformation mechanism [7]. For example, a value of $n = 1.5$ is expected for diffusion-controlled growth in three dimensions of particles, on the assumption that all embryos are present at the start. If the particles nucleate at a constant rate and grow via diffusion-controlled growth, an n value of 2.5 is expected [7].

The figure shows a gradual change in slope as the aging progresses from $n \approx 1.3$ to $n \approx 0.5$. The initial slope is consistent with three-dimensional diffusion-controlled growth of the β phase, with most of the nucleation sites active from the start of the transformation. This is reasonable because the samples were powders. However, when the surfaces of the powders are completely covered with the new phase, only one-dimensional growth can occur (into the grains). Thus the slope decreases to about one-half. This seems to begin after about 2.5 h.

It should be noted that this curve shows the fraction of β phase transformed and is not a plot of the homogeneous decomposition of the α phase. Also the fact that the data were taken from powder specimens of small particle size must be kept in mind when interpreting the data since the free surface enhances the heterogeneous component of the transformation. For example, Figs. 2(a) and 2(b) are micrographs of large-grained samples. In both of these cases there is *less* β phase formed for the given time than the plot in Fig. 1 suggests. These figures show that the formation of β phase starts at grain boundaries (Fig. 2(a)), inclusions or free surfaces (Fig. 2(b)). There are four variants of the β phase observed in Fig. 2(b).

Figure 3 shows the progression of the homogeneous decomposition, as observed by TEM. The microstructure is consistent with

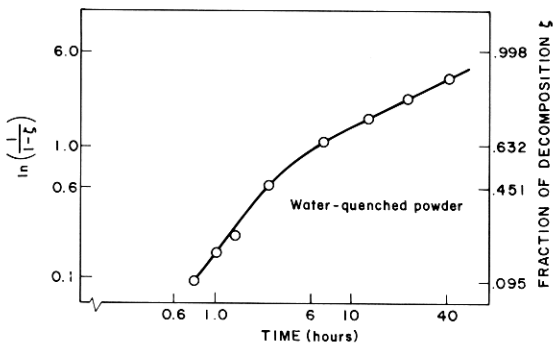

Fig. 1. The volume fraction of β phase formed in a water-quenched powder sample as a function of aging time at room temperature: $\zeta = 1 - \exp(-Kt^n)$.

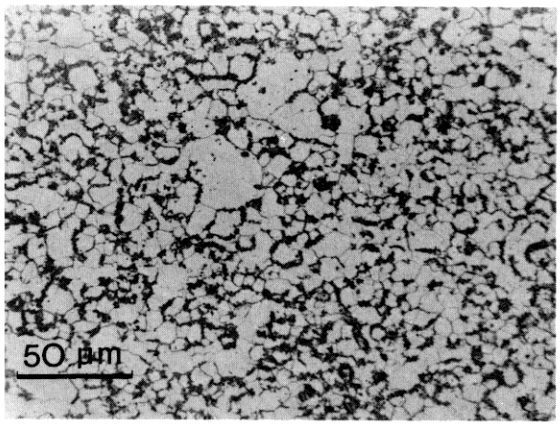

(a)

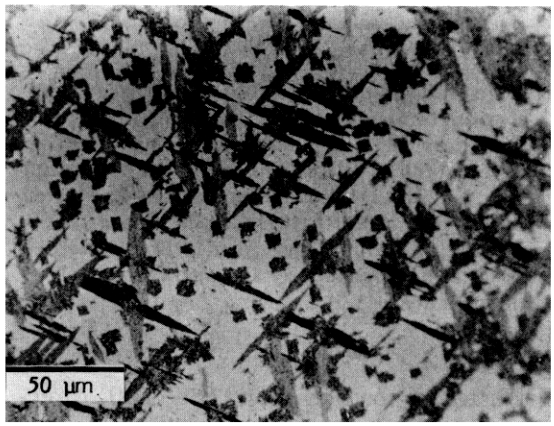

(b)

Fig. 2. (a) A photomicrograph of a sample taken 2 h after quenching from 350 °C (the heterogeneous transformation product at the grain boundaries should be noted); (b) a photomicrograph of a sample taken 2 days after quenching from 350 °C (the photograph was taken within a very large grain; the heterogeneous transformation at the inclusion should be noted).

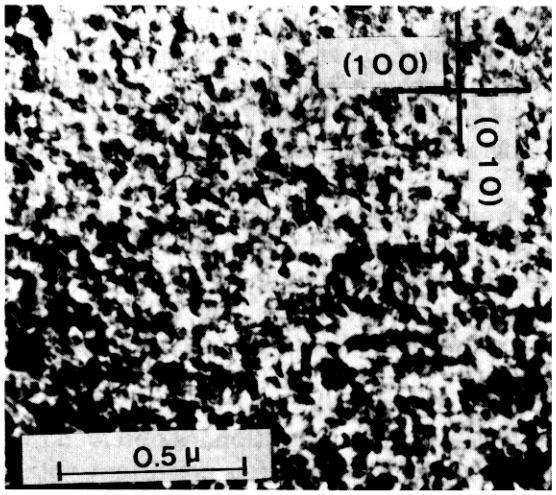

(a)

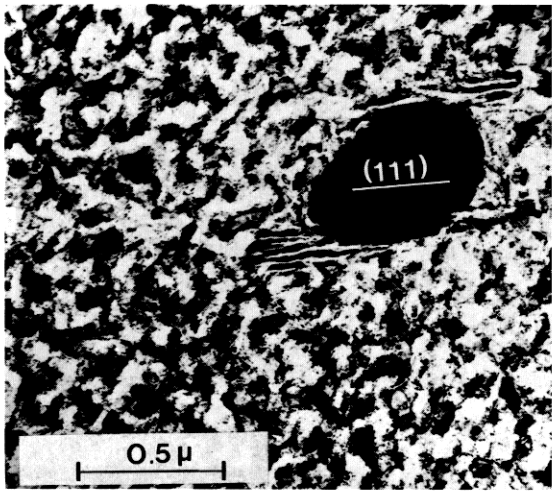

(b)

Fig. 3. (a) A TEM micrograph of a sample aged for 7 h at room temperature after water quenching from 350 °C (the modulations along the ⟨100⟩ directions should be noted); (b) a TEM micrograph of a sample aged for 2 months at room temperature after water quenching from 350 °C (it should be noted that decomposition products are formed both heterogeneously and homogeneously and also that the ⟨100⟩ alignment is absent).

initial decomposition along the ⟨100⟩ directions (Fig. 3(a)). It should be noted that the contrast is produced by coherency strains. This transformation could not be studied quantitatively by X-rays because the α reflections were very close to the parent α' reflections. The presence of the heterogeneously formed β phase at an inclusion in Fig. 3(b) should be noted.

3.2. X-ray line broadening

Typical plots of $(B\cos\theta)/\lambda$ against $(\sin\theta)/\lambda$ which are used for the calculation of the crystallite size (α or β phase formed by the homogeneous transformation) and the internal stress are shown in Figs. 4 and 5 for samples aged for 6 days and 2 months respectively. The scatter of the data, which are taken from the breadth of various reflection lines, is due to the crystallite shape (non-equiaxed) and the anisotropy of the elastic constant of the phases.

The results of the crystallite size and internal stress measurements for various heat-treated and cold-worked samples are summarized in Table 1. No internal stress is detectable in samples subjected to aging for up to 6 days; during this time period the "crystallite" size is shown to be extremely small, about 300 Å. The internal stress in samples aged for 2 months is surprisingly high and has the same order of magnitude as the yield strength of the alloy.

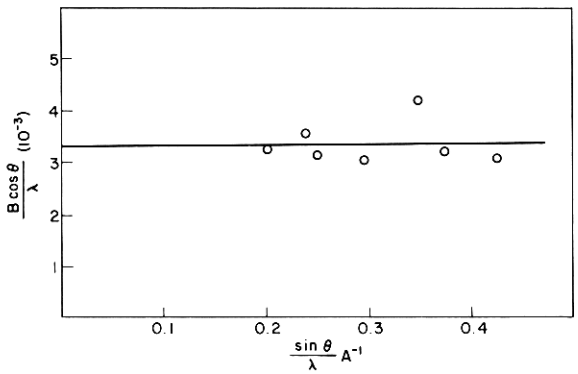

Fig. 4. A plot of $(B\cos\theta)/\lambda$ against $(\sin\theta)/\lambda$ for a sample aged for 6 days at room temperature after water quenching from 350 °C.

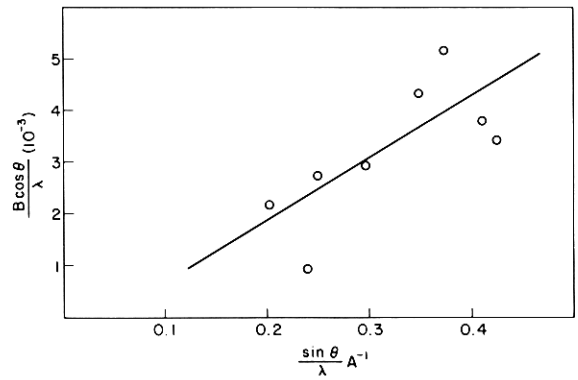

Fig. 5. A plot of $(B\cos\theta)/\lambda$ against $(\sin\theta)/\lambda$ for a sample aged for 2 months at room temperature after quenching from 350 °C.

TABLE 1

Crystallite size and internal stress of various samples measured by X-ray line broadening

Sample	*Crystallite size* (Å)	*Internal stress* (lbf in^{-2} (MPa))
68 h after quench	270	0 (0)
6 days after quench	300	0 (0)
2 months after quench	> 2000[a]	73000 (503)
Quenched and cold rolled	1400	25000 (172)
As-filed powder[b]	600	15000 (103)

[a] The crystallite size is too large to measure using this technique.
[b] Filed from the commercial sheet, measured within 1 h after filing.

3.3. *Mechanical properties*

The results of tensile and hardness tests as a function of time at room temperature after quenching from above the eutectoid temperatures are shown in Fig. 6. The material hardened significantly with aging time as a result of eutectoid decomposition. It is interesting that, although the strength increases more than twofold, the tensile elongation (at fracture) remains approximately the same.

Figure 7 shows the load–elongation curves of samples aged for various times. The as-quenched sample showed a low strength because it is a single phase. The material exhibited considerable work hardening and fractured in rather a brittle fashion with very little necking. The fully transformed samples have high yield strengths; however, they exhibited negative work-hardening coefficients. This two-phase material fractured in a ductile fashion with significant necking. The

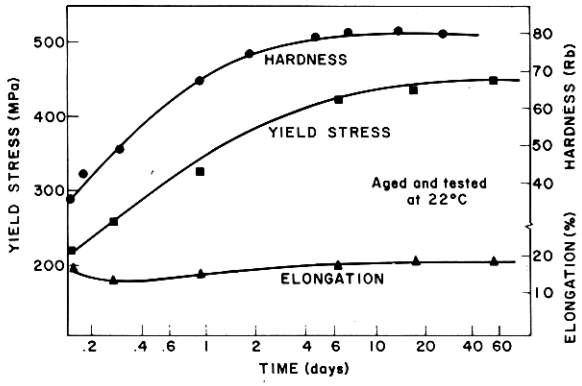

Fig. 6. Hardness, yield stress and elongation shown as functions of the aging time at room temperature after water quenching from 350 °C.

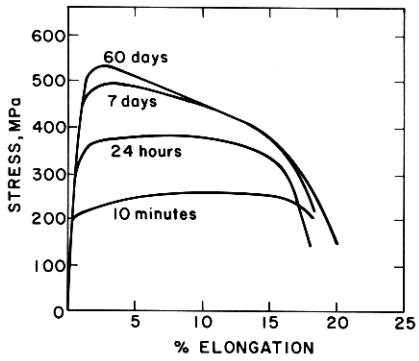

Fig. 7. Stress–strain curves of samples aged for various times at room temperature.

relative ductility of the samples can also be observed by fractography. Figures 8(a) and 8(b) are fractographs of samples fractured after aging for 10 min and 60 days respectively at

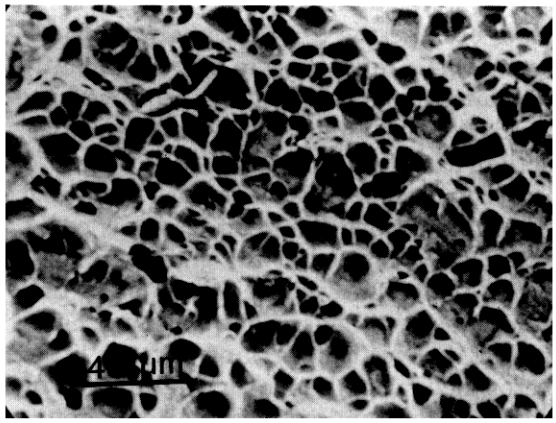

(a)

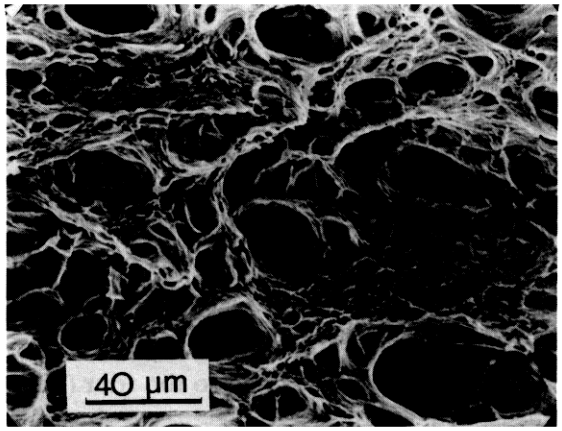

(b)

Fig. 8. SEM fractographs of a sample tested in tension after (a) 10 min and (b) 60 days of aging at room temperature.

room temperature. The sample aged for 60 days appears to fracture in a more ductile fashion.

4. DISCUSSION

There are two transformations occurring at room temperature: a heterogeneous transformation and a homogeneous transformation. The former starts at grain boundaries, inclusions and surfaces. The latter occurs throughout α' grains, producing a coherent two-phase structure within them. This reaction can be written as

$$\alpha' \rightarrow \alpha_1 + \alpha_2$$

The α_1 phase eventually becomes α, and the α_2 phase eventually becomes β.

Only the kinetics of the heterogeneous reaction were studied by X-ray diffraction. This is because the α reflections were too close to the α' reflections to perform quantitative intensity measurements. However, the "powders" accentuated the heterogeneous reaction, as did the free surfaces of the optical microscopy samples. For example, under the optical microscope the heterogeneous component which started at the grain boundary (see Fig. 2) was shown to cover much of the surface area 2 - 4 days after quenching; however, TEM investigation showed very little heterogeneous component in the interior of specimens decomposed at room temperature for a comparable time. Therefore the degree of transformation for the water-quenched sample shown in Fig. 1 has been enhanced by the heterogeneous surface component.

Careful examination of the surface–inclusion heterogeneous component shown in Fig. 2(b) reveals four variants, indicating an epitaxial relationship between the α' matrix and the decomposed phases. This tendency to form on special planes is also observed in the TEM photograph shown in Fig. 3(b) in that the lamellae at both sides of the inclusion are parallel. A previous study indicated that the homogeneously formed β phase also had four variants which corresponded to the four (111) planes in the α' phase [1].

It is very interesting to see that although no internal stress could be detected by X-rays in samples aged for 6 days (at 22 °C) the hardness and tensile data showed significant strengthening within only 1 day of aging. The initial strengthening shown in the mechanical tests is therefore most probably due to the crystallite size strengthening, as it is of the order of 300 Å. As the aging time increases, the crystallite size strengthening decreases, while the internal stress increases. The grain boundary sliding may play an important role in the deformation of the fully decomposed sample. Deformation may have destroyed the coherency of the two phases and produced a fine-grained structure at the neck, resulting in a more ductile fracture [1].

The internal stress in the sample 2 months after quenching has approximately the same order of magnitude as the tensile strength. This high internal stress combined with compositional inhomogeneity and/or casting defects explains the cracking observed in the continuous cast slab during room temperature aging.

Cold working immediately after quenching from above the eutectoid temperature produces less internal stress (see Table 1). This is because the heterogeneous component enhanced by the presence of dislocations prevails and/or the residue dislocations relieve part of the coherency strains.

The stress–strain curves are of interest, exhibiting either positive or negative work-hardening coefficients, depending on the microstructure and the degree of decomposition. We believe that the work hardening and brittle fracture is due to the partial eutectoid decomposition which occurred during deformation. Dislocations generated by deformation serve as nucleation sites for the heterogeneous decomposition during the tensile test. This hinders the dislocations from gliding, explaining the work hardening and brittle fracture observed (see Figs. 7 and 8(a)). The fact that the β phase forms so quickly at room temperature during deformation was also observed on samples that were quenched from solutionizing temperatures, immediately cold rolled and examined by X-ray diffraction. Such samples always had more than 20% of the β reaction completed.

In contrast, deformation in the fully decomposed material (deformed after 60 days at room temperature) has destroyed the coherency strain by transforming the coherent phase boundaries into incoherent ones. Thus the work hardening is negative. The material

fractured in a ductile fashion because grain boundary sliding, especially at the neck, may have played an important role. The dimples shown in the fractograph of the fully aged sample (Fig. 8(b)) confirm that the material fractured in a ductile fashion.

5. CONCLUSIONS

This investigation enabled us to explain various mechanical properties of this commercial Al–Zn alloy in terms of phase transformations and resulting microstructures. The following can be concluded with respect to the processing and use of the alloy.

(1) The alloy transformed at room temperature produces an internal stress about equal to the yield strength of the material. This, combined with mechanical and/or chemical defects of the casting, induces cracking of the as-cast ingot. Therefore prolonged natural aging of the as-cast ingot should be avoided.

(2) Although water quenching from above the eutectoid temperature considerably improves the tensile strength of the material compared with as-rolled samples or samples air-cooled from above the eutectoid temperature, the negative work hardening makes the material unattractive for structural application.

ACKNOWLEDGMENTS

The authors would like to thank Mingyu Hwang, Kathleen Brunner and Roberto Rioja for technical assistance throughout the project.

Permission for publication by the management of St. Joe Minerals Corporation is gratefully appreciated.

Support from the Materials Research Laboratory Section, Division of Materials Research, National Science Foundation, through the use of central research facilities is also gratefully acknowledged.

REFERENCES

1 F. W. Ling and D. E. Laughlin, *Metall. Trans. A, 10* (1979) 921.
2 T. L. Bartel and K. B. Rundman, *Metall. Trans. A, 6* (1975) 1887.
3 A. J. Perry, *Acta Metall., 14* (1966) 1143.
4 F. W. Ling, *Proc. Symp. on Thermomechanical Processing of Aluminum Alloys*, Metallurgical Society of the AIME, St. Louis, MO, 1978.
5 F. W. Ling, unpublished research, 1978.
6 A. Taylor, *X-ray Metallography*, Wiley, New York, 1961.
7 R. W. Cahn, *Physical Metallurgy*, North-Holland, New York, 1965.